Structures of the N^{ω}-Hydroxy-L-Arginine Complex of Inducible Nitric Oxide Synthase Oxygenase Dimer with Active and Inactive Pterins[†,‡]

Brian R. Crane,[§,||] Andrew S. Arvai,[§] Sanjay Ghosh,[⊥] Elizabeth D. Getzoff,[§] Dennis J. Stuehr,[⊥] and John A. Tainer*[,§]

The Department of Molecular Biology and The Skaggs Institute for Chemical Biology, The Scripps Research Institute, La Jolla, California 92037, and The Department of Immunology, The Cleveland Clinic, Cleveland, OH, 44106

Received October 18, 1999; Revised Manuscript Received December 17, 1999

ABSTRACT: Nitric oxide synthases (NOSs) catalyze two mechanistically distinct, tetrahydrobiopterin (H_4B)-dependent, heme-based oxidations that first convert L-arginine (L-Arg) to N^{ω}-hydroxy-L-arginine (NHA) and then NHA to L-citrulline and nitric oxide. Structures of the murine inducible NOS oxygenase domain ($iNOS_{ox}$) complexed with NHA indicate that NHA and L-Arg both bind with the same conformation adjacent to the heme iron and neither interacts directly with it nor with H_4B. Steric restriction of dioxygen binding to the heme in the NHA complex suggests either small conformational adjustments in the ternary complex or a concerted reaction of dioxygen with NHA and the heme iron. Interactions of the NHA hydroxyl with active center β-structure and the heme ring polarize and distort the hydroxyguanidinium to increase substrate reactivity. Steric constraints in the active center rule against superoxo-iron accepting a hydrogen atom from the NHA hydroxyl in their initial reaction, but support an Fe(III)-peroxo-NHA radical conjugate as an intermediate. However, our structures do not exclude an oxo-iron intermediate participating in either L-Arg or NHA oxidation. Identical binding modes for active H_4B, the inactive quinonoid-dihydrobiopterin (q-H_2B), and inactive 4-amino-H_4B indicate that conformational differences cannot explain pterin inactivity. Different redox and/or protonation states of q-H_2B and 4-amino-H_4B relative to H_4B likely affect their ability to electronically influence the heme and/or undergo redox reactions during NOS catalysis. On the basis of these structures, we propose a testable mechanism where neutral H_4B transfers both an electron and a 3,4-amide proton to the heme during the first step of NO synthesis.

In the biological production of nitric oxide, nitric oxide synthases (NOSs) catalyze the 5-electron heme-based oxidation of L-arginine (L-Arg) to L-citrulline (L-Cit) via the stable intermediate N^{ω}-hydroxy-L-arginine (NHA)[1] (*1*). In the first step, L-Arg is hydroxylated to N^{ω}-hydroxy-L-arginine (NHA) by a mixed function oxidation (*2*−*4*) analogous to reactions catalyzed by the cytochrome P-450s (*5, 6*). In this reaction, a proposed oxo-iron intermediate (P•−Fe(IV)═O where P• is a porphyrin or protein radical) is thought to abstract a hydrogen atom from substrate and then rapidly recombine with the resulting radical to form the hydroxylated product. In the second step of the NOS reaction, evidence suggests that a one-electron oxidation of NHA by superoxo-iron (P−Fe(III)−OO^-) produces an NHA radical that is subsequently attacked by peroxo-iron (P−Fe(III)−OO^{2-}) (*1, 7, 8*). The iron-peroxo-NHA radical intermediate formed by this nucleophilic addition could then collapse to NO and L-Cit (*9, 10*). Structures of catalytically competent NOS with bound substrates and intermediates are important to resolve the mechanism of O_2 activation and reactivity in each step of NO synthesis.

NOSs are found in three homodimeric isozymes: inducible NOS (iNOS), neuronal NOS (nNOS), and endothelial NOS (eNOS). Each NOS isozyme contains a catalytic N-terminal oxygenase domain (NOS_{ox}, residues 1−498 for iNOS) that binds heme (iron protoporphyrin IX), tetrahydrobiopterin ((6*R*,1′*R*,2′*S*)-5,6,7,8-tetrahydrobiopterin or H_4B), and substrate L-Arg, and a C-terminal electron-supplying reductase domain (NOS_{red}, residues 531−1144 for iNOS) that is homologous to cytochrome P-450 reductase and binds flavin mononucleotide (FMN) (*3, 4*), flavin adenine dinucleotide (FAD), and NADPH. An intervening calmodulin-binding region (residues 499−530 for iNOS) regulates reduction of NOS_{ox} by NOS_{red} (*4, 11*). Isolated oxygenase domains are fully competent for NO synthesis when suitable electron donors are provided.

[†] Supported by National Institute of Health Grants HL58883 (E.D.G.) and CA53914 (D.J.S.), fellowship grants from the Helen Hay Whitney Foundation (B.R.C.), and the Skaggs Institute for Research (A.S.A. and B.R.C.).

[‡] PDB codes for the structures reported within: NHA−H_4B, 1DWX; NHA−H_2B, 1DWW; NHA−4-amino-H_4B, 1DWV.

[§] The Scripps Research Institute.

[||] Present address: The Beckman Institute, The California Institute of Technology, Pasadena California 91125

[⊥] The Cleveland Clinic.

* To whom correspondence should be addressed. Telephone: (858)-784-8119. Fax: (858)784-2289. E-mail: jat@scripps.edu.

[1] Abbreviations: DHFR, dihydrofolate reductase; eNOS, endothelial nitric oxide synthase; 4-amino-H_4B, (6*R*,1′*R*,2′*S*)-4-amino-5,6,7,8-tetrahydrobiopterin; H_2B, (6*R*,1′*R*,2′*S*)-7,8 dihydrobiopterin; H_4B, (6*R*,1′*R*,2′*S*)-5,6,7,8-tetrahydrobiopterin; $iNOS_{ox}$, inducible nitric oxide synthase oxygenase domain; L-Arg, L-arginine; L-Cit, L-citrulline; NHA, N^{ω}-hydroxy-L-arginine; nNOS, neuronal nitric oxide synthase; NO, nitric oxide; NOS, nitric oxide synthase; q-H_2B, quinonoid dihydrobiopterin; Scit, L-thiocitrulline.

10.1021/bi992409a CCC: $19.00
Published on Web 03/31/2000

High sequence conservation among all three NOS isozymes and high structural similarity between $iNOS_{ox}$ and $eNOS_{ox}$ (*12*−*15*) suggest the isozymes have essentially the same catalytic mechanisms. Structures have been determined for complexes of NOS_{ox} with the substrate L-Arg, the product analogue thiocitrulline (Scit), and S-ethyl-isothiourea (*12*−*14*). Partial hydroxylation of L-Arg was characterized in the substrate complex of $eNOS_{ox}$, but the mechanistic implications of the NHA complex were not discussed (*14*). Because NHA is the product of the first reaction and the substrate for the second, its structure in the NOS active center will impact the potential mechanisms for both steps of NOS catalysis. Furthermore, the compatibility of the NHA conformation with heme-bound dioxygen constrains possibilities for NOS heme oxygen chemistry.

Despite extensive research into the function of H_4B in NOS catalysis, the role of the pterin remains puzzling (*2, 3, 11, 16*). Although H_4B can stabilize the dimeric states of all NOS isozymes (*11, 17*−*20*), it is clearly more than an allosteric activator (*2, 3, 11, 16*) and recent studies suggest it may be a redox-active cofactor (*21*). We originally identified a hydrogen bonding interaction between the pterin 3,4-amide and a heme propionate group as being key for the ability of H_4B to influence heme reactivity (*12*). To further address structural coupling between H_4B and the heme and the role of pterin in NOS catalysis, we herein report the crystal structure determinations of $iNOS_{ox}$ complexed with the reaction intermediate NHA and either the active pterin H_4B, the inactive oxidized pterin dihydrobiopterin H_2B (*22, 23*), or the inactive tetrahydropterin 4-amino-H_4B (*24*).

EXPERIMENTAL PROCEDURES

Materials. NHA was obtained from Alexis, H_4B from Sigma, H_2B from Dr. B. Schirck's laboratory (Jona, Switzerland), and 4-amino H_4B as a kind gift from B. Mayer (Universität Graz, Austria). All other chemicals were from Sigma unless otherwise noted.

Protein Purification and Crystallization. Murine $iNOS_{ox}$ Δ65 (residues 66−498) with a fused C-terminal 6-His tag was overexpressed in *Escherichia coli* and purified in the absence of pterin or substrate by using Ni-chelate chromatography as described previously (*25*). Hexagonal $iNOS_{ox}$ Δ65 crystals of space group $P6_122$ (cell dimensions 213.0 × 213.0 × 114.2 Å^3, two molecules/asymmetric unit, Matthews coefficient (V_M) = 4.0, solvent content = 70%) were grown by vapor diffusion as reported previously (*12*). Briefly, drops contained an equal volume mixture of crystallization reservoir and 17 mg/mL $iNOS_{ox}$ Δ65 in 40 mM *N*-(2-hydroxyethyl)piperazine-*N*′-(3-propane sulfonic acid) (HEPPS), pH 7.6, 10% glycerol, 1 mM dithiothreitol, 4 mM NHA, and either 2 mM H_4B, 2 mM 4-amino-H_4B, or 200 μM H_2B. The reservoir was composed of 50 mM 2-(*N*-morpholino)ethanesulfonic acid (MES), pH 5.5−6.5, 50 mM β-octyl-glucoside and 18−21% Li_2SO_4 or $(NH_4)_2SO_4$. Crystals were grown at 4 °C and flash frozen for data collection within 2 days. Because of the limited stability of soluble H_4B not bound to NOS, we have also collected diffraction data on $iNOS_{ox}$ crystals soaked in 10 mM fresh H_4B an hour prior to data collection. The structures determined from short-soaking experiments show no change in pterin or protein conformation compared to structures determined from crystals grown in the presence of pterin.[2]

Structure Determination and Refinement. The crystals for both structures were isomorphous with previously determined $iNOS_{ox}$ structures (*12*). Diffraction data were collected at 100 K with synchrotron radiation from the Stanford Synchrotron Radiation Laboratory and the Advanced Light Source. The data sets were reduced with DENZO (*26*) and scaled with SCALEPACK (*26*). XFIT (*27*) was used for model building and structural analysis, while all refinement of crystallographic models was carried out with X-PLOR (*28*) and CNS (*29*). For the structure determination, a previously refined model of $iNOS_{ox}$ Δ65 to 2.6 Å resolution (*12*), with pterin, ligands, and water molecules removed, was used for initial bulk solvent and overall anisotropic temperature factor corrections. The structures were then refined by positional refinement in X-PLOR against the new diffraction data, first to 3.2 Å, then to 2.6 Å, and finally to the extent of the data resolution. In all data sets, the same 5% of the reflections were set aside for R_{Free} calculation. The loops and areas surrounding the active center and NOS zinc site were rebuilt to $F_o - F_c$ omit electron density maps, whereas the rest of the molecule, which changed little in conformation, was surveyed and adjusted with standard $F_{obs} - F_{calc}$ and $2F_{obs} - F_{calc}$ maps. Ligands were modeled into the resulting difference peaks on the distal side of the heme, and water molecules were added gradually over cycles of positional conjugate gradient refinement followed by *B*-factor refinement. Noncrystallographic symmetry restraints were maintained on 70% of the backbone atoms in the two nonidentical subunits for the 2.6 Å resolution H_4B-containing structure, but released for the 2.35 Å resolution H_2B- and 4-amino-H_4B-containing structures. Water molecules were placed only in difference peaks greater than 3 σ that were 2.2−3.5 Å from appropriate protein hydrogen-bonding partners.

Molecular Modeling of the Dioxygen−Iron-NHA Ternary Complex and a Covalent Intermediate. Superoxo-iron and peroxo-iron were modeled into the active center of the H_4B−NHA structure with XFIT (*27*). Parameters for the bond lengths and angles were taken for superoxo-iron from the structure of superoxo-cytochrome *c* peroxidase (CCP) complex (*30*) and for peroxo-iron from ab initio and molecular dynamics calculations (*31, 32*). In the dioxygen complexes, the heme iron is assumed to be low spin and in the plane of the pyrrole nitrogens. The small structural difference between superoxo-iron and peroxo-iron resides mainly in the Fe−O−O angle (130° for superoxo-iron, 120° for peroxo-iron). We originally considered both end-on ($^1\eta$) and bridging ($^2\eta$) binding of peroxide to the heme iron. Although synthetic ferric porphyrins likely bind peroxide in a bridging geometry (*33, 34*), a trans axial ligand (e.g., the NOS proximal thiolate) promotes an open, end-on binding mode and increases nucleophilicity (*35*). Furthermore, calculations on peroxide complexes with peroxidase and cytochrome P-450 hemes strongly argue against bridging mode binding (*31, 32, 36*). The structure of a heme protein−peroxide complex is not known, but in CCP Fe(III)$-O_2^-$ binds end-on (*30*).

[2] We have also determined structures of $iNOS_{ox}$ complexed with a proprietary inhibitor and H_4B, H_2B, or 4-amino-H_4B to 2.15, 2.0, and 2.15 Å resolution, respectively (unpublished data). These higher resolution structures, which will be published separately as a drug design study, confirm the pterin conformations observed in the NHA complexes.

Table 1: Data Collection and Refinement Statistics for the $iNOS_{ox}$−NHA Complex with H_4B, H_2B, and 4-Amino-H_4B

structure	NHA, H_4B	NHA, H_2B	NHA, 4-amino H_4B
scatterers	7236	7766	7461
residues	2×(77−101, 108−496)	2×(77−496)	2×(77−496)
cofactors	2×(1Hem, $1H_4B$)	2×(1Hem, $1H_2B$)	2×(1Hem, 4-amino H_4B)
ions	1 SO_4^{2-}	2×(4 SO_4^{2-}), $1Zn^{2+}$	2×(4 SO_4^{2-}), $1Zn^{2+}$
disulfides	1	0	0
ligands	2×NHA	2×NHA	2×NHA
waters	352	729	423
resolution	30.0−2.6 Å (2.72−2.60 Å)[a]	30.0−2.35 Å (2.43−2.35 Å)[a]	30.0−2.35 Å (2.43−2.35 Å)[a]
unique reflections	46622	62465	58616
observations	153562	303449	212755
% completeness	97.8 (88.1)[a]	98.7 (96.7)[a]	92.3 (76.5)[a]
$\langle I/\sigma I\rangle$[b]	18.6 (2.8)[a]	28.9 (7.4)[a]	28.2 (5.2)[a]
R_{sym} (%)[c]	5.7 (32.8)[a]	7.4 (28.9)[a]	5.2 (28.2)[a]
R (%)[d]	23.8 (37.5)[a]	24.9 (37.5)[a]	24.7 (37.2)[a]
free R(%)[e]	27.8 (42.5)[a]	28.8 (41.4)[a]	28.6 (38.1)[a]
⟨overall B⟩ (Å^2)[f]	49.7	52.8	60.8
⟨main chain B⟩ (Å^2)	49.4	50.6	59.4
⟨side chain B⟩ (Å^2)	51.6	52.1	61.3
rms bnd (Å)[g]	0.008	0.009	0.009
rms ang (deg)[g]	1.4	1.4	1.4

[a] Highest resolution bin for compiling statistics. [b] Intensity signal-to-noise ratio. [c] $R_{sym} = \sum\sum_j|I_j - \langle I\rangle|/\sum\sum_j I_j$. [d] $R = \sum||F_{obs}| - |F_{calc}||/\sum|F_{obs}|$ for all reflections (no σ cutoff). [e] Free R calculated against 5% of the reflections removed at random. The same free reflections were chosen for all three structures. [f] Overall model average thermal (B) factor followed in parentheses by estimated B factor from Wilson scaling. [g] Root mean square deviations from bond and angle restraints.

A structure of a putative iron-peroxo-NHA radical intermediate was modeled in the $iNOS_{ox}$ active center and minimized with X-PLOR (*28*) using parameters determined from ab initio calculations (*7*). We aimed to test if this tetrahedral intermediate could be sterically accommodated in the $iNOS_{ox}$ active center and thus only geometric restraints and van der Waals interactions were applied in the minimization.

RESULTS

We determined three crystallographic structures (Table 1) of the $iNOS_{ox}$ dimer complexed with its reaction intermediate NHA and either its cofactor H_4B or inactive cofactor analogues (H_2B or 4-amino H_4B). To the resolutions at which they are characterized, these NHA complexes with active and inactive pterins are essentially identical (Table 1); this has profound implications for understanding NOS heme-oxygen chemistry and pterin function in both L-Arg and NHA oxidation.

NOS Active Center Structure with Bound NHA. Active center conformational change does not accompany conversion of substrate L-Arg to intermediate NHA in the first step of NOS catalysis. The highest resolution structure of the NHA complex (2.35 Å, with H_2B) clearly reveals that the NOS active center conformation with bound intermediate (Figures 1 and 2A) is very similar to that with bound substrate. NOS_{ox} dimers consist of two identical subunits, each with a central winged β-structure surrounded by α-helices that associate at an extensive dimer interface involving both amino and carboxy-terminal elements of the subunit polypeptide (*12*, *37*). The deep active center channel in NOS begins near the dimer interface and leads to the substrate-binding site beside the heme (Figure 1). The protein β-structure frames the Cys194-ligated heme and stacks NHA, like L-Arg, between the porphyrin and surrounding hydrophobic residues (Figure 2 A and B). The NHA hydroxyguanidinium resides at the bottom of the active center channel, sandwiched between Pro344 and the heme, whereas the NHA amino acid groups interact with polar residues positioned toward the dimer interface (Figures 1 and 2). In NOS, the heme is substantially distorted from planarity. The B and C pyrrole rings, situated at the back of the heme pocket, bend up and away from the proximal thiolate by ∼20° relative to a plane defined by the A and D pyrrole rings. The heme is also saddled with the A and C meso carbons directed up from the proximal thiolate and the B and D meso carbons directed down. In the NHA−H_2B complex, the 24 atoms defining the porphyrin deviate ∼0.15 Å on average from planarity and the high-spin Fe(III) domes toward the proximal thiolate by ∼0.35 Å from the pyrrole nitrogen plane.

Identical hydrogen bonds from NOS to the like atoms of L-Arg and NHA suggest that only the L-Arg nitrogen directed toward the heme participates in the hydroxylation reaction. The NHA bridging hydroxyguanidino nitrogen (NE) hydrogen bonds to Glu371, whereas the terminal nitrogen (NH1) hydrogen bonds to both Glu371 and the peptide carbonyl of Trp366. The oxime nitrogen (N^{ω}) projects toward the center of the porphyrin, ∼4.0 Å away from the heme iron (Figure 2A). The NHA amino group hydrogen bonds with the same heme propionate that interacts with the pterin and Glu371, whereas the carboxylate group interacts with Tyr367, Gln257, and Asp376, which is likely protonated to satisfy its hydrogen bond partners (*12*). The only major difference between the binding modes of NHA and L-Arg in the active center results from the addition of the NHA hydroxyl.

The NOS active center provides a special environment for the NHA hydroxyl that likely promotes the conversion of NHA to L-Cit and NO. The hydroxyl group of NHA extends toward the base of the heme pocket in a direction aligned with the Fe−CHC (mesocarbon) vector, but does not coordinate the heme iron (Figure 2 A and B). The Gly365 peptide nitrogen, contained on β-strand 9b (see refs *12* and *37* for nomenclature) at the back of the heme pocket, is in

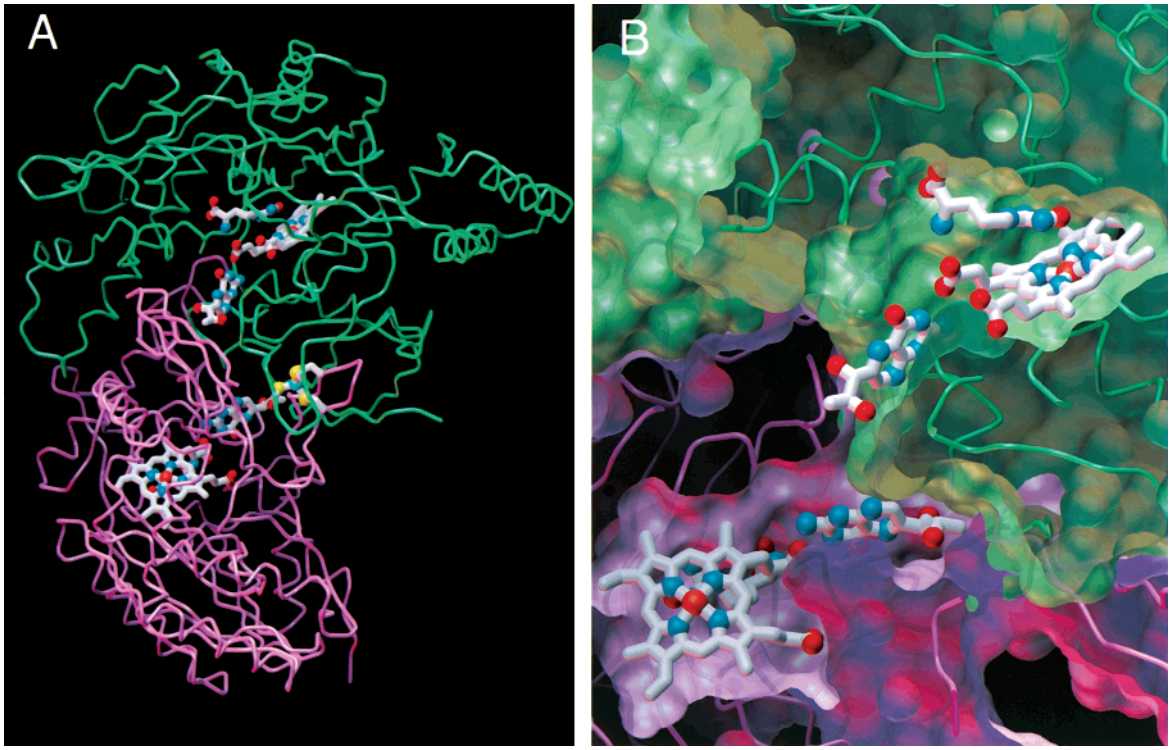

FIGURE 1: (A) Cα trace of the $iNOS_{ox}$ dimer (green and magenta subunits) showing the relative positioning of the two hemes (center of top and bottom subunits, red oxygen atoms, blue nitrogen atoms, orange iron atoms, gray carbon bonds), two reaction intermediates NHA (above and below heme planes), and the two pterins (center, back and front). A large active center channel leads from the surface of the molecule near the dimer interface, past the pterin, to the heme pocket where NHA binds adjacent to the heme iron. The subunits are covalently linked by a symmetrical tetrathiolate zinc site (right, yellow sulfur atoms, and cyan zinc atom) at the dimer interface. (B) Solvent-accessible surfaces of the cofactor binding sites and dimer interface in $iNOS_{ox}$ (close up of the same orientation as in (A)).

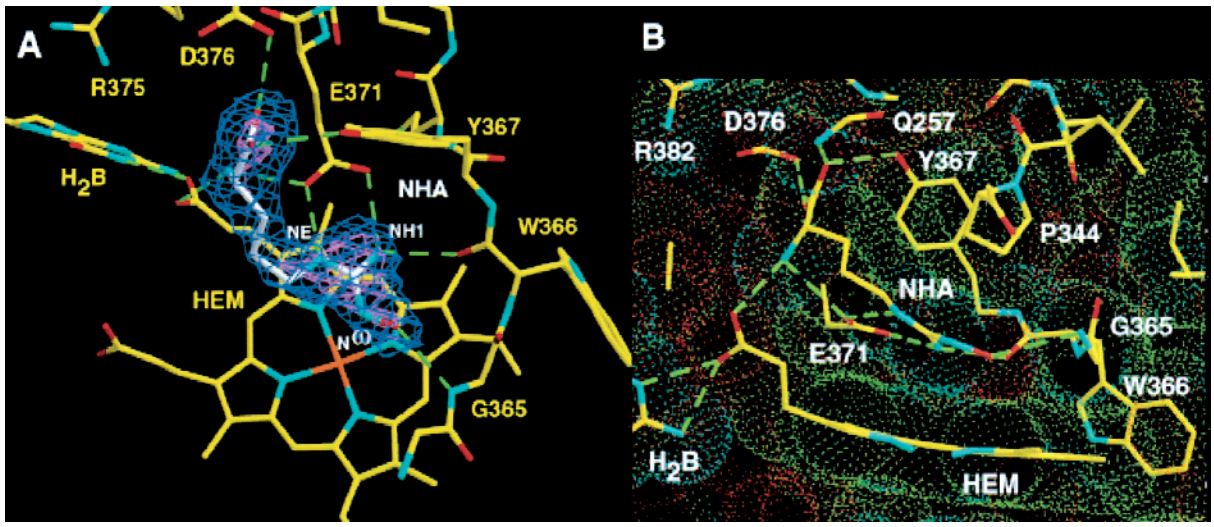

FIGURE 2: (A) NHA bound in the active center of $iNOS_{ox}$ complexed with H_2B. 2.35 Å simulated-annealed $F_o - F_c$ omit map (contour levels shown at 3σ for blue and 6σ for magenta) showing electron density for NHA in the $iNOS_{ox}$ active center. NHA (white carbon atoms, blue nitrogen atoms, red oxygen atoms) stacks overtop of the heme (yellow carbon atoms, orange iron atom) with nitrogens NE and NH1 hydrogen bonding (green lines) to Glu371 and the carbonyl of Trp366. The remaining NHA nitrogen (N^{ω}) projects toward the heme iron and its attached hydroxyl group hydrogen bonds to Gly365 peptide nitrogen. The amino acid moiety of NHA hydrogen bonds to Tyr367, Asp376, Gln257 (not shown), Glu371, and the same heme carboxylate as H_2B (or H_4B) interacts with. (B) van der Waals interactions (dotted surfaces) in the $iNOS_{ox}$ active center. The NHA hydroxyl oxygen (red) is distorted out of the plane of the NHA guanidinium group by protonation of N^{ω} or packing against the bent $iNOS_{ox}$ heme. Hydrogen bonding interactions of NHA are shown as in (A).

hydrogen bonding distance (3.1 Å) of the NHA hydroxyl. Although the Gly365 peptide nitrogen also points toward the Pro344 peptide carbonyl on β-strand 8b, the separation between donor and acceptor is 4.0 Å due to the spread between β8 and β9 caused by the winged β-sheet. Thus, the unique NOS β-structure may allow the Gly365 backbone amide to provide electrostatic complementation and possibly polarization for the NHA hydroxyl through a hydrogen bonding interaction.

The NHA hydroxyl is tightly constrained at the bottom of the heme pocket. In fact, when the NHA hydroxyguanidine is held planar during crystallographic refinement, the hydroxyl is forced within 2.8 Å of a heme pyrrole nitrogen, extremely close for a van der Waals contact. Refinement

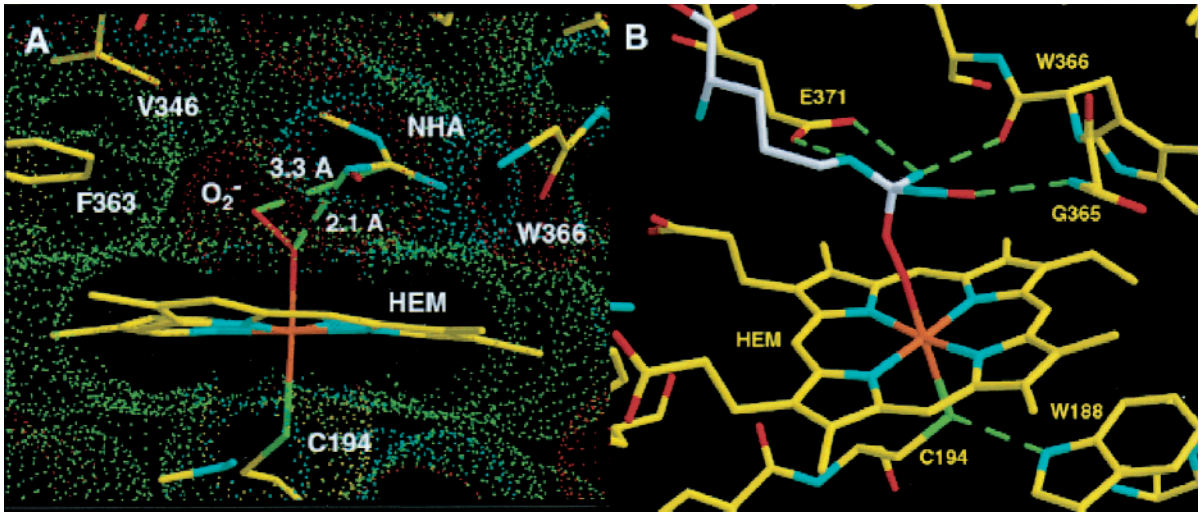

FIGURE 3: (A) Model of a $iNOS_{ox}$ ternary complex with bound NHA and superoxide coordinated to the heme iron. The terminal superoxy oxygen (red with dotted van der Waals surface) can only be accommodated in a pocket formed by V345, F363, and NHA. A close contact between the iron-coordinated oxygen and the NHA nitrogen suggests that some readjustment in the active center is necessary for dioxygen and NHA to bind simultaneously. (B) Minimized model of a putative Fe(III)−peroxo−NHA tetrahedral intermediate in the NOS_{ox} active center. Tetrahedral distortion of the central hydroxyguanidinium carbon in the intermediate improves the alignment of the hydrogen bond between the hydroxyl and the Gly365 peptide nitrogen.

with the hydroxyguanidine planarity unrestrained bends the NHA hydroxyl 8−10° from the guanidinium plane to match omit map electron density. Similar deviations from planarity are observed in small molecule crystal structures of hydroxyguanidinium cations (*38*, *39*). Thus, at the pH of our crystals (∼6.0), the NHA N^{ω} may be protonated and pyramidalized. The NHA hydroxyl hydrogen is likely positioned between the carbonyl groups of Gly365 and Trp366 to allow hydrogen bonding between the NHA hydroxyl oxygen and the Gly365 peptide nitrogen. There are no protein-supplied bases in proximity of the NHA hydroxyl that could catalyze its deprotonation.

Structural Restrictions on a NOS Ternary Complex with NHA and Dioxygen. The NHA-bound $iNOS_{ox}$ structures highly constrain the placement of heme-bound dioxygen relative to NHA in a ternary complex. In the NOS active center, superoxo-iron and NHA react with NOS to form products; peroxo-iron and an NHA radical have been proposed as intermediates in this reaction (*9*, *10*). NHA in the NOS active center allows only one possible conformation of dioxygen (Figure 3A) when dioxygen is coordinated in an end-on binding mode to the heme iron. The terminal superoxo or peroxo oxygen can reside without steric constraint only in a small pocket bordered by NHA, Pro344, and Val346. The separation between central hydroxyguanidinium carbon and the terminal dioxygen oxygen would be ∼3.3 Å for superoxide and ∼3.6 Å for peroxide; the larger separation with peroxo-iron being due to its larger Fe−O−O bond angle. Importantly, the terminal superoxo-oxygen is over 4.0 Å from the NHA hydroxyl proton. Thus, hydrogen atom transfer between superoxo oxygen and the NHA hydroxyl seems unlikely in this model.

Steric clash between the heme-bound oxygen and NHA indicates that some adjustment of the substrate or the heme is needed to simultaneously accommodate both reactants in the active center. Iron coordination to reduced dioxygen forces the iron-bound oxygen within 2.1 Å of NHA N^{ω}. Sufficient space for nearby residues to adopt alternate side-chain conformations is not apparent, although small shifts of the heme, NHA, and/or surrounding β-structure could probably provide an additional 1 Å of separation. Moreover, the unfavorable contact could be avoided without protein shifts if a concerted reaction among NHA, dioxygen, and the reduced heme forms a covalent conjugate during oxygen heme ligation.

Despite steric constraint in the NHA−dioxygen ternary complex, a model for the proposed iron-peroxo-NHA radical intermediate (*9*, *10*) is well-accommodated in the NOS active center (Figure 3B). Either superoxo-iron or peroxo-iron could swivel around their respective Fe−O bonds for addition to the NHA central guanidinium carbon and formation of a covalent tetrahedral intermediate. This species has reasonable geometry and van der Waals contacts in the NOS active center and maintains the hydrogen bonds of NHA with the protein (Figure 3B). Close contacts of the dioxygen in the ternary complex are avoided by bond formation with the NHA hydroxyguanidine and its distortion toward tetrahedral geometry. Moreover, improved alignment of the hydrogen bond between NHA hydroxy and the Gly365 peptide amide in the tetrahedral intermediate compared to the NHA complex suggests that the active center structure favors progression toward this species. Thus, our models indicate that although modest structural shifts are needed to simultaneously accommodate dioxygen and NHA in the NOS active center, the proposed iron-peroxo-NHA radical intermediate is structurally reasonable when extrapolated from the NHA complex.

NHA-bound NOS with Active and Inactive Pterins. Surprisingly, substitutions of the naturally occurring, catalytically active H_4B with inactive pterins H_2B and 4-amino-H_4B do not produce significant measurable changes in $iNOS_{ox}$ or the pterins themselves (Figure 4), at the resolutions of our enzyme structures (Table 1). Thus, the differences in NOS activity associated with these pterin-bound enzymes cannot be attributed to protein conformational changes nor to different pterin-binding modes. Simulated-annealing omit maps, calculated with NHA and pterins removed, confirmed that the three structures are virtually identical in the active

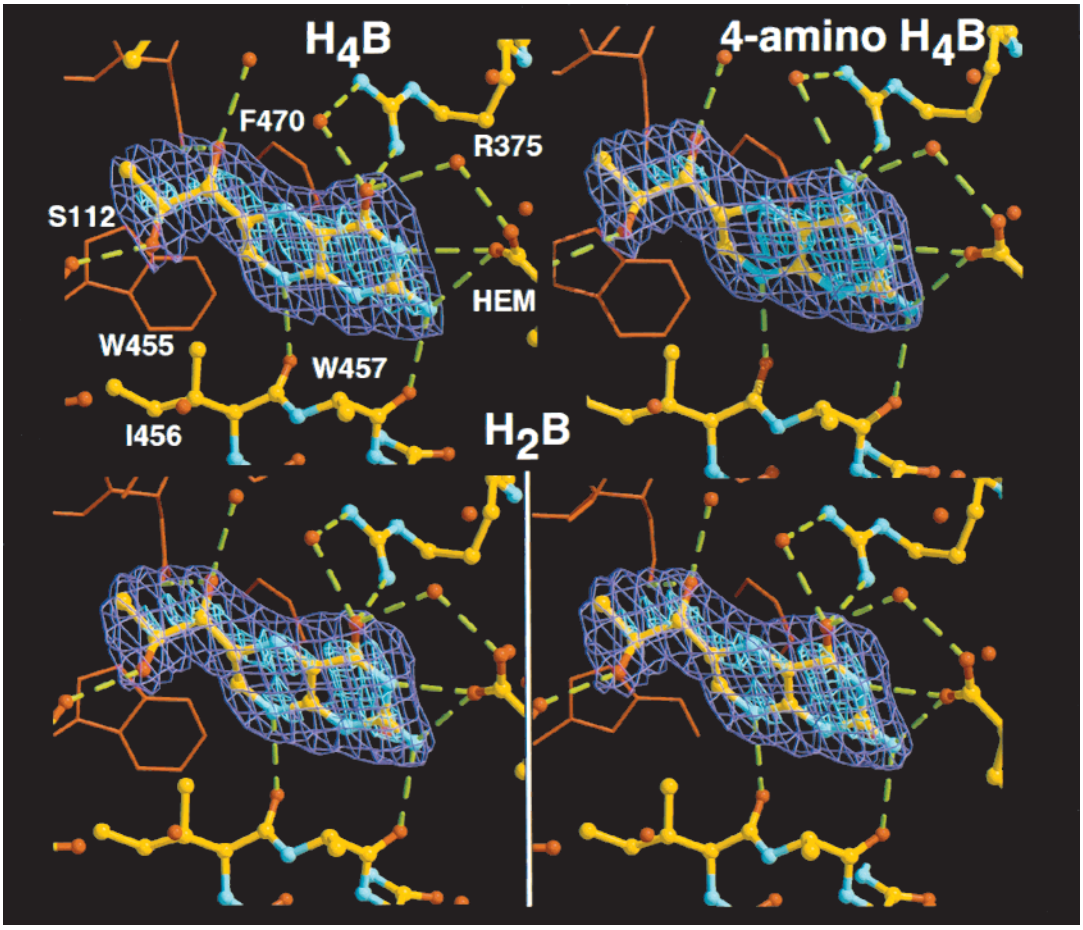

FIGURE 4: Pterin-binding to $iNOS_{ox}$. Simulated-annealed omit maps showing electron density for either H_4B (top left, 2.6 Å resolution, 4σ purple contours and 8σ for cyan contours), 4-amino-H_4B (top right, 2.35 Å resolution, 4.5σ purple contours and 8σ for cyan contours) or H_2B (bottom left and right stereopair, 2.35 Å resolution, 4.5σ purple contours and 8σ for cyan contours), in the $iNOS_{ox}$ active center. H_4B, H_2B, and 4-amino-H_4B make identical hydrogen bonds (green lines) with $iNOS_{ox}$ residues and water molecules (red spheres). The hydrogen bonding interactions to the heme carboxylate are likely essential for NO synthesis. The pterins bind at the dimer interface and stack between Trp458 (not shown) and Trp455 and Phe470 of the adjacent subunit (red bonds).

centers (Figure 4), and $F_{obs} - F_{calc}$ difference maps calculated between each pair of the three structures reveal no significant difference peaks near the pterins.

In all cases, two pterins of the $iNOS_{ox}$ dimer bind at the dimer interface, about 13 Å apart (measured between C7 carbon atoms) and 40° from coplanarity (Figure 1). Hydrogen bonding and hydrophobic packing structurally couple the pterin sites to each other, to the heme and heme-bound ligand, and to secondary structural elements participating in the dimer interface (Figure 1). Each H_4B pteridine ring resides below the heme ring relative to the substrate-binding site and hydrogen bonds to the same heme propionate as the L-Arg amino group. H_4B, H_2B, and 4-amino-H_4B maintain the π-stacking interactions with Trp457 of one subunit and Trp455 and Phe470 of the opposite subunit, as described previously (*12*, *40*). Mutation of these residues to nonaromatics reduces not only pterin affinity but also NO synthesis activity in the presence of saturating pterin (*40*). All three pterins also make identical hydrogen bonds to the protein, including those from N3 and N4 of the pteridine ring to the heme carboxylate (Figures 4 and 5). However, because the three pterins have different oxidation states and favored tautomers, the hydrogen bonding interactions provided by the protein have different implications for the possible protonation states of each pterin (Figure 5).

In our structure, H_2B evidently binds primarily in the quinonoid form (q-H_2B, Figure 5B). This is especially surprising given that the 7,8-dihydro form (7,8-H_2B Figure 5B), which is favored in solution, was used in producing the $iNOS_{ox}$ crystals. Notably, the side chain position relative to the pyrazine ring differs in 7,8-H_2B compared to q-H_2B, due to the geometry about C6, which is trigonal planar in 7,8-H_2B, instead of tetrahedral in q-H_2B and H_4B. When H_2B is refined as 7,8-H_2B in $iNOS_{ox}$, a positive $F_{obs} - F_{calc}$ difference peak near C6 suggests that the side chain is not modeled correctly relative to the ring. Omit map electron density (Figure 4) indicates that the dihydropropyl side chain in H_2B is oriented analogously to the side chain in H_4B. Furthermore, no difference peaks are present close to the pterin when diffraction data from the H_4B and H_2B complexes are compared. This observation is also consistent with our other higher resolution structures containing H_4B or H_2B (unpublished results[2]). To test for possible conversion of H_2B to H_4B by dismutation or dithiothreitol reduction we assayed the same $iNOS_{ox}$ sample used for crystallization with full-length pterin-free iNOS. No activity of full-length iNOS was found in assays sensitive to <10% conversion of H_2B to H_4B. Furthermore, we find no detectable H_4B when millimolar concentrations of H_2B are incubated under conditions identical to those that produced our crystals. Thus, our

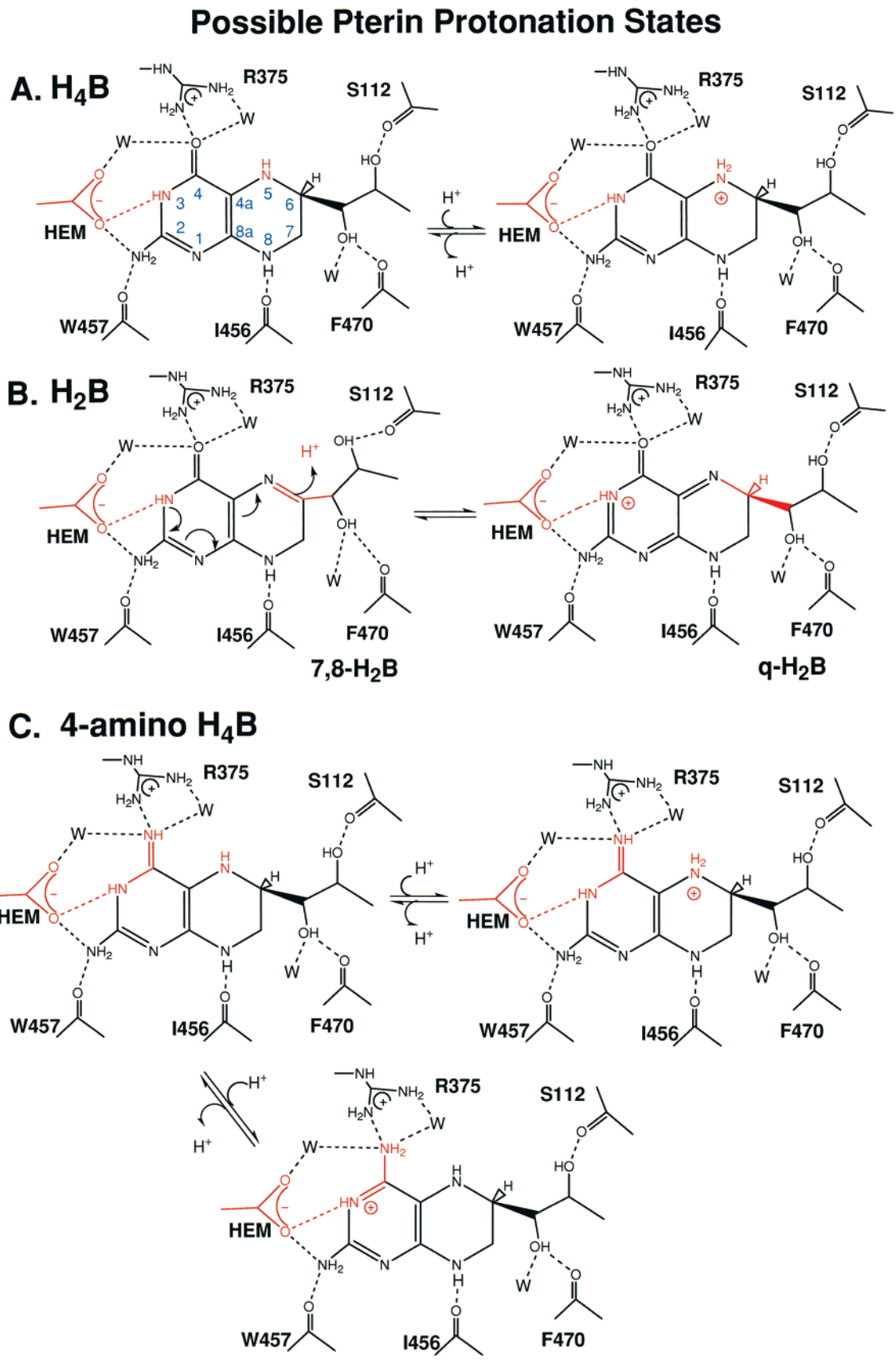

FIGURE 5: Possible protonation states for H_4B, H_2B, and 4-amino-H_4B based on hydrogen bonding patterns in the $iNOS_{ox}$ active center. H_4B could bind neutral or singly charged by proton addition to N5. However, only N3 protonation allows charged H_2B to satisfy its protein hydrogen bond acceptors when bound in the quinonoid form (right). Acid catalysis by the heme carboxylate may convert 7,8-H_2B to q-H_2B in the NOS active center. Our structures do not distinguish if the proton is localized on the heme carboxylate or pterin N3. Similarly, the most favorable tautomer of 4-amino-H_4B is also likely charged and protonated at N3 when bound to $iNOS_{ox}$.

crystals contain primarily H_2B bound as the quinonoid (q-H_2B) with C6(H) tetrahedral and hydrogenated. Moreover, q-H_2B maintains the native hydrogen bond between the heme propionate and N3, even though N3 of q-H_2B is not protonated in the neutral form of q-H_2B. This hydrogen bond implies that either q-H_2B becomes positively charged to satisfy all of the protein hydrogen bond acceptors or that the heme carboxylate is protonated and neutral (Figure 5B).

Similarly, our $iNOS_{ox}$ structure with 4-amino-H_4B shows that this inactive reduced (tetrahydro) pterin, like the inactive oxidized (dihydro) pterin H_2B, is likely protonated at N3 and positively charged within the protein. Although the most stable form of neutral 4-amino-H_4B in solution would have an amino (not imino) group at position N4, leaving N3 unprotonated, the 4-amino-H_4B $iNOS_{ox}$ structure maintains a hydrogen bond between N3, and the heme carboxylate (Figure 5C). As described above for H_2B, this hydrogen bond in $iNOS_{ox}$ implies that either 4-amino-H_4B becomes positively charged (Figure 5C) or that the heme carboxylate is protonated and neutral. Substitution of the 4-hydroxo position of the pteridine ring with an amino group raises the pterin pK_a 1.1 units in solution (*41*), making protonation of 4-amino-H_4B more favorable than protonation of H_4B. Thus, our different pterin-loaded $iNOS_{ox}$ structures support a change in the charged state of protein-bound pterin for neutral H_4B compared to protonated H_2B or 4-amino-H_4B. Protonation would affect the ability of pterin to undergo redox chemistry or to tune the reactivity of the NOS iron-oxy complex, thereby providing an explanation for $iNOS_{ox}$ inactivity, despite structural similarity.

DISCUSSION

A primary goal of bioinorganic chemistry is to understand how enzymes achieve a wide variety of oxidative chemistry by employing different forms of metal-activated oxygen. NOS is particularly interesting, because its heme active center catalyzes two mechanistically distinct oxidations of the similar substrates L-Arg and NHA. Furthermore, despite similarities between the heme chemistry of NOS and the cytochromes P-450, NOS catalysis requires the additional cofactor H_4B in each step of NO synthesis. Analyses of three structures of NHA-bound $iNOS_{ox}$ dimer with different pterins probe structural constraints on NOS catalysis. Below, we consider the implications of these new structures for catalytic mechanism and pterin function in each step of NOS catalysis.

The First Step of NO Synthesis: L-Arg Oxidation to NHA. The similarities among the structures of the substrate L-Arg (*12*), intermediate NHA, and product analogue Scit (*12*) bound in the $iNOS_{ox}$ active center suggest that catalysis could occur without significant conformational changes in the active center. In fact, with the exception of the additional interactions of the NHA hydroxyl, L-Arg, NHA, and Scit make the same hydrogen bonding interactions with the enzyme. In the first step of NO synthesis, an activated oxygenspecies formed from the heme-based two-electron reduction of oxygen hydroxylates one guanidino nitrogen of L-Arg. The close proximity of one L-Arg nitrogen (N^{ω}) to the heme iron (~4.0 Å) and the similarity of the reaction to monooxygenations of P-450s suggest that NOS catalysis proceeds via a putative oxo-iron intermediate that reacts solely with N^{ω}. Because of the absence of an ionizable residue near the heme iron, we have previously suggested that L-Arg itself donates a proton to heme-bound oxygen to facilitate O−O bond scission (*12*). Proton and/or electron donation by the substrate or intermediate to the heme−oxygen complex may be an essential controlling feature in both steps of NOS catalysis.

The Second Step of NO Synthesis: NHA One-Electron Oxidation. The structure of the $iNOS_{ox}$−NHA complex constrains possible mechanisms for NHA oxidation in the NOS active center. Formation of NO and L-Cit from NHA requires the formal one-electron oxidation of NHA by superoxo-iron (*1, 21, 42*−*44*). In fact, superoxide alone can convert N-hydroxyguanidines to urea-derivatives and nitric oxides in microsomal (*45*−*47*) and chemical systems (*48*). In the NOS reaction, hydrogen atom transfer from NHA to superoxo-iron was proposed for the initial oxidation of NHA based on thermodynamics (*8*) and the ability of N-hydroxyguanidine to transfer a hydrogen atom to suitable acceptors (*49*). However, our structures indicate that the steric constraints on simultaneously binding dioxygen and NHA place the terminal oxygen of an dioxygen−iron species distant from the NHA hydroxyl and poorly oriented to receive a hydrogen atom. Barring significant conformational rearrangement in the active center, the terminal oxygen and NHA hydroxyl hydrogen would be separated by over 4 Å. In contrast, NHA nitrogen N^{ω} is better situated to donate a hydrogen atom or proton to the heme−oxygen complex. Protonation of N^{ω} is consistent with the observed N^{ω} pyramidalization and 10° distortion of the NHA hydroxyl from the guanidinium plane. N^{ω} protonation would also imply that NHA (pK_a ~8.1 [*50*]) is positively charged in our NOS crystals, because NH1 of NHA must have two protons to satisfy hydrogen bonds with the Glu371 carboxylate and the Trp366 carbonyl.

ENDOR spectroscopy found evidence for only one exchangeable proton on NHA within 5.3 Å of the heme iron and within 5−10° from the heme normal (*51*). Our structures indicate that the NHA hydroxyl proton is positioned 4.5−4.8 Å from the heme iron and 20° from the heme normal, in agreement the ENDOR-derived distance of 4.8 Å, but larger than the ENDOR-derived angle (5−10°). By comparison, a proton on N^{ω} would fall within 5−10° of the heme normal, as predicted by ENDOR, but closer (<4.0 Å) to the heme iron. Importantly, N^{ω} protonation would place two exchangeable protons within 5.3 Å of the heme iron, an interpretation consistent with our structures and worth reevaluation by ENDOR. Although the pH of our crystals (~6.0) is lower than that of the ENDOR experiments (7.4, refs *51* and *52*), the steric contraints in the NOS active center disfavor accommodation of a completely planar hydroxyguanidine. Thus, the position and geometry of the NHA hydroxyl suggest that the superoxo-iron does not accept a hydrogen atom from the NHA hydroxyl, but may accept a proton from N^{ω}. Alternatively, if NHA is neutral when bound to NOS at higher pH, concerted free-radical addition of superoxide to NHA (*53*) may produce a peroxo-iron−NHA radical conjugate without formal electron or proton transfer from NHA to heme-bound oxygen (Figure 6A, bottom arrow).

The Second Step of NO Synthesis: Breakdown of the NHA Radical. Either reaction of peroxo-iron with an NHA radical or reaction of superoxo-iron with NHA will lead to a peroxo-iron−NHA radical conjugate (Figure 6A, central panel).

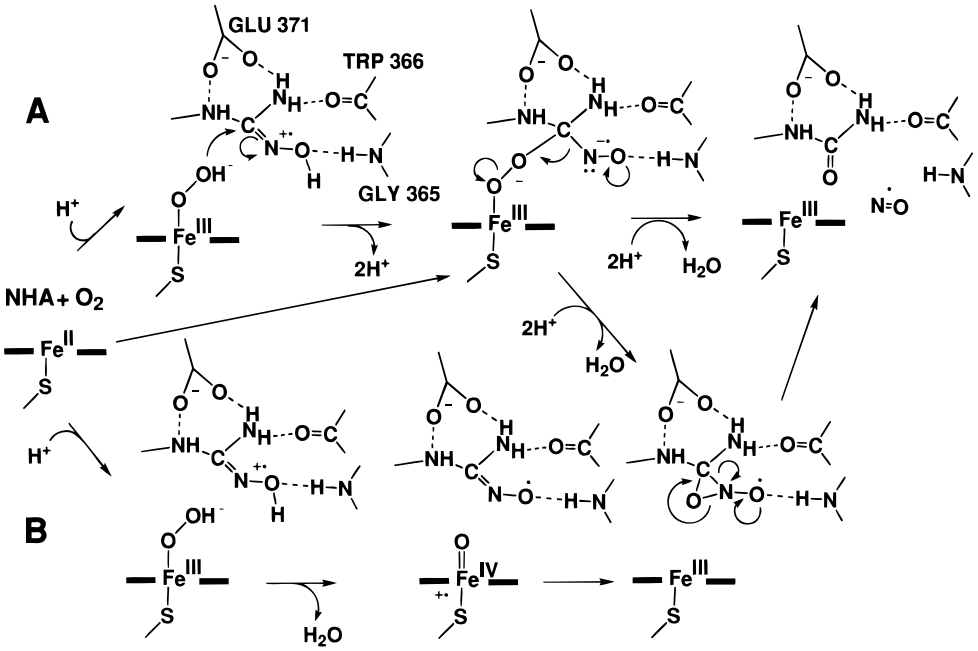

FIGURE 6: Possible mechanisms for NHA oxidation by $iNOS_{ox}$. In scheme A, a nucleophilic peroxo-iron, formed from O_2 binding to Fe(II) and NHA oxidation, attacks the central carbon of the NHA radical and forms a covalent intermediate that then breaks down to NO and citrulline. Breakdown of the intermediate could also occur via an oxaziridine, as shown in frame 3 of scheme B. A concerted reaction of dioxygen with NHA and the Fe(II) could also lead to the central panel of A without requiring formation of an NHA radical or proton transfer to heme-bound oxygen (bottom arrow in A). In scheme (B), peroxo-iron first breaks down to a high-valent iron-oxo species, which reacts with the NHA oxime to form an oxaziridine (frame 3). The oxziridine opens to produce NO and citrulline. NHA^+ may donate the initial proton to superoxo-iron in either mechanism A or B.

Specific features of the $iNOS_{ox}$−NHA structure support a mechanism that proceeds through this intermediate and its subsequent breakdown to L-Cit and NO. First, the Gly365 peptide nitrogen near the NHA hydroxyl apparently polarizes the NHA oxime toward a nitrosyl group. Such polarization would facilitate addition by superoxo- or peroxo-iron and nitrosyl release on collapse of the ensuing tetrahedral intermediate. Second, the NHA hydroxyguanidinium may be distorted by either N^{ω} protonation or close contact with the heme. Bending of the hydroxyl out of the guanidinium plane would destabilize the substrate toward peroxo-iron conjugation (Figure 2B) and favor release of the nitrosyl group. Furthermore, the Gly365 peptide nitrogen is better aligned to hydrogen bond with the nitrosyl in the tetrahedral intermediate than in the NHA complex. Thus, the architecture of the β-structure surrounding the heme pocket in NOS appears optimized for catalyzing the breakdown of NHA by raising the energy of the ground state and stabilizing the transition state.

Alternatively, if superoxo-iron does formally oxidize NHA, our structures do not discount high-valent oxo-iron participating in the second step of the reaction (Figure 6B). In fact, oxo-iron formation would be facilitated by proton donation from NHA N^{ω}. Furthermore, oxo-iron would be well-situated relative to the NHA oxime to form an oxaziridine, which could ring open to produce L-Cit and NO (Figure 6B). Oxaziridine formation has been proposed to explain the additional production of cyanoornithine and NO^- from NHA when the NOS reaction is shunted with peroxide (*54*). In this mechanism, peroxide reacts directly with the heme to form an oxo-iron intermediate, which then adds to the NHA oxime (*54*). The absence of cyanoornithine formation in the natural reaction was taken to rule against oxo-iron formation in favor of peroxo-iron; however, an NHA-derived oxaziridine could also form via peroxo-iron (Figure 6, arrow linking scheme A to B). If both mechanisms proceed through an oxaziridine, then the lack of cyanoornithine production in the natural reaction could be explained by the different reactivity of the oxidized NHA radical compared to neutral NHA in the peroxide-shunted reaction. Although an oxo-iron would avoid the close contact predicted between a heme-bound peroxide and the NHA oxime nitrogen, dioxygen must still initially bind with NHA in the pocket to produce oxo-iron. Thus, the close contact between the heme-bound oxygen and NHA N^{ω} predicted in our ternary complex model (Figure 3A) does not necessarily favor the reaction proceeding through an oxo intermediate. Recent spectral evidence indicates that an FeO_2 species does form in NHA-bound NOS prior to oxidation of NHA (*92*). Flattening of the heme, or slight shifts in the active center could extend the modeled 2.1 Å separation between the NHA N^{ω} and bound dioxygen by at least 1 Å. Significantly, our structures suggest how an oxo-iron could act in both steps of NO synthesis.

The Role of Pterin in NOS Catalysis is more than Structural. Although H_4B was the first NOS cofactor identified, its role in NOS catalysis remains elusive. H_4B stabilizes the dimeric form of all NOS enzymes to varying extents (*2, 11*). H_4B-binding promotes dimerization, heme sequestration, and conformational change in the interface region of iNOS (*17, 55*−*57*), but the eNOS dimer is not influenced to the same extent (*58*). In nNOS, pterin binding is synergistic with substrate binding and the two pterin sites can behave anticooperatively (*2, 18*). In vivo, pterin availability influences monomer/dimer ratios in iNOS and membrane-bound eNOS (*20, 55, 59*). These effects of pterin in NOS isozymes have a strong structural basis, because H_4B binds directly at the dimer interface, the two pterin sites share structural elements, and there is an extensive hydrogen

bonding network integrating the pterin sites with the heme and the substrate-binding sites (*12, 14*). Direct interactions of H_4B with iNOS and eNOS are virtually identical (*12*−*14*). Large structural changes occur in the pterin-binding regions of monomeric $iNOS_{ox}$ Δ114 compared to the dimeric enzyme (*12, 37*). Although Raman et al. reported no structural changes between the $eNOS_{ox}$ with and without pterin bound (*13*), the binding site for the H_4B dihydroxypropyl side chain was occupied by glycerol in the pterin-free structure, and the pterin site may have been further stabilized by influence of the crystal lattice on the $eNOS_{ox}$ dimer. Pterin also helps sequester the heme-coordinating cysteine from solvent. The thiolate environment is likely key for preventing heme dissociation during product inhibition by NO (*60*) and for controlling the reactivity of the heme−oxygen complex (*61*). Yet, the inability of close H_4B analogues to support NO synthesis (*2, 22, 23*) and increase the autoxidation rate of the ferrous−dioxygen complex (Abu-Soud, H. M., and Stuehr, D. J., unpublished data) suggests a specific role for H_4B in catalysis beyond its significant structural influences.

Oxidized pterin (dihydrobiopterin or H_2B) does not support NHA production; in fact, tetrahydropterins seem essential for NO synthesis (*23*). However, the tetrahydropterin 4-amino-H_4B, which stabilizes the NOS dimer much like H_4B, does not support NO synthesis from either L-Arg or NHA (*24, 62, 63*). Importantly, the activity of the 5-methyl analogue of H_4B rules out reductive O_2 activation by the pterin cofactor (*64*). Furthermore, the structures of NOS_{ox} complexes with L-Arg and NHA clearly demonstrate that H_4B does not react directly with either of these substrates. Thus, in addition to its structural roles, pterin must act as a redox cofactor or modifier of heme reactivity in NOS catalysis, but the nature of this action has remained enigmatic.

H_4B is positioned to influence the electronic state of the heme in a manner that could include direct electron-transfer (*12, 13*). Yet, all evidence suggests that the reducing equivalents necessary for NOS catalysis ultimately originate from NADPH (*3*) and can be derived from FMN semiquinone (*65*). Furthermore, flavin-dependent heme reduction by NOS_{red} occurs in the absence of H_4B, and the rate of initial heme iron reduction in H_4B-free iNOS is actually equal to or slightly faster than the rate in H_4B-saturated NOS (*23*). However, this does not discount H_4B as the source for the second electron delivered to the oxygen−iron complex during L-Arg hydroxylation. Recent evidence suggests that one-electron reduced NOS_{ox} can acquire a second electron (presumably from H_4B) to convert L-Arg to NHA (*21*). Yet, in single turnover experiments of nNOS at 37 °C, this reaction did not occur to a significant extent (*44*). If the reduced tetrahydro oxidation state of H_4B is necessary for NO synthesis, then the inactivity of 4-amino-H_4B is surprising, considering that its reduction potential is likely not much different than that of H_4B and 5-methyl-H_4B (*66*), both of which are active pterins.

Protonation States of NOS-bound Pterins Affect Their Ability to Support Catalysis. The surprisingly identical binding modes, hydrogen bonding interactions, and surrounding water structure among the three pterin complexes indicate that structural perturbation is not responsible for the inactivity of H_2B or 4-amino-H_4B. The electron density maps for the NOS−H_2B complex suggest that H_2B binds as the quinonoid, because of pyrazine ring nonplanarity and dihydroxypropyl side chain position. Binding of q-H_2B was unexpected, because the crystals were soaked with 7,8-H_2B, which is much more stable in solution (*67*−*71*). However, hydrogen bonding interactions and packing contacts with the protein favor the dihydroxypropyl side chain conformation of H_4B in NOS (Figure 4), consistent with large changes in pterin affinity for NOS upon modification of the pterin side chain (*22, 23*). Thus, increased stability in NOS of q-H_2B, which closely resembles H_4B, may favor the quinonoid isomer in the binding pocket. Importantly, binding of q-H_2B implies that the either the N3 amide or the heme carboxylate must be protonated to satisfy the protein hydrogen bond acceptors (Figure 5). In solution, acid−base catalysis converts q-H_2B to 7,8-H_2B and then results in hydrate formation and side chain loss (*68*−*71*). The NOS heme carboxylate could correspondingly act as a base to catalyze tautomerism to the quinonoid form (Figure 5B). Thus, when bound to NOS, H_2B differs from H_4B in its oxidation and protonation state.

In contrast, the only significant difference between active H_4B and inactive 4-amino-H_4B when bound to NOS is the pterin charge and/or where that charge is localized on the pteridine ring (Figure 5). The most likely protonation state of 4-amino-H_4B that satisfies all of the protein hydrogen bonding patterns in the $iNOS_{ox}$−H_4B complex has an N4 amino (rather than imino) function and N3 protonated for hydrogen bonding with the heme carboxylate. Protonation of H_4B at 3,4-amide is not necessary for interaction with the heme carboxylate. It has been suggested that H_4B binds NOS positively charged, because N5 protonation (Figure 5B) increases stability of this state against autoxidation and because of the ability of positively charged L-Arg to substitute for H_4B in a pterin-depleted $eNOS_{ox}$ (*13*). If N3 of 4-amino-H_4B is protonated to maintain the hydrogen bond with the heme carboxylate, then it is unlikely that N5 is also protonated, because this would produce a +2 charge on the pterin. If N5 of 4-amino-H_4B is not protonated when bound to NOS, then N5 of H_4B may not be either. Unfortunately, protons are undetectable at the resolution of our structures, and there are insufficient protein hydrogen-bond partners to distinguish the protonation state of N5 for any of these three pterins (Figure 4). The higher solution pK_a of the 4-amino-H_4B (6.7) (*72*) compared to that of H_4B (5.6) (*41*) would favor protonation of 4-amino-H_4B over H_4B, but the lower pK_as of 7,8-H_2B (4.2) (*41*) or q-H_2B (∼5) (*70*) would not. However, the pK_as of the biopterins when bound to $iNOS_{ox}$ may be perturbed to favor their preferred binding modes. A more positive charge on the pterin or heme could raise the redox potential of either or both cofactors due to pterin interactions with the heme carboxylate. An increased heme redox potential may reflect the inability of H_2B and 4-amino-H_4B to accelerate decay of the ferrous-oxy species (Abu-Soud, H. M., and Stuehr, D. J., unpublished results).

The structures presented here indicate that H_4B likely binds NOS neutral and 4-amino-H_4B likely binds NOS protonated; we propose that this difference could be solely responsible for the inactivity of 4-amino-H_4B. Despite no apparent structural differences between the H_4B and 4-amino-H_4B NOS complexes, 4-amino-H_4B has a 20× higher binding affinity for the enzyme (*24*). This increased affinity is likely due to an increased positive charge on 4-amino-H_4B compared to H_4B. An increased affinity of protonated 4-amino-

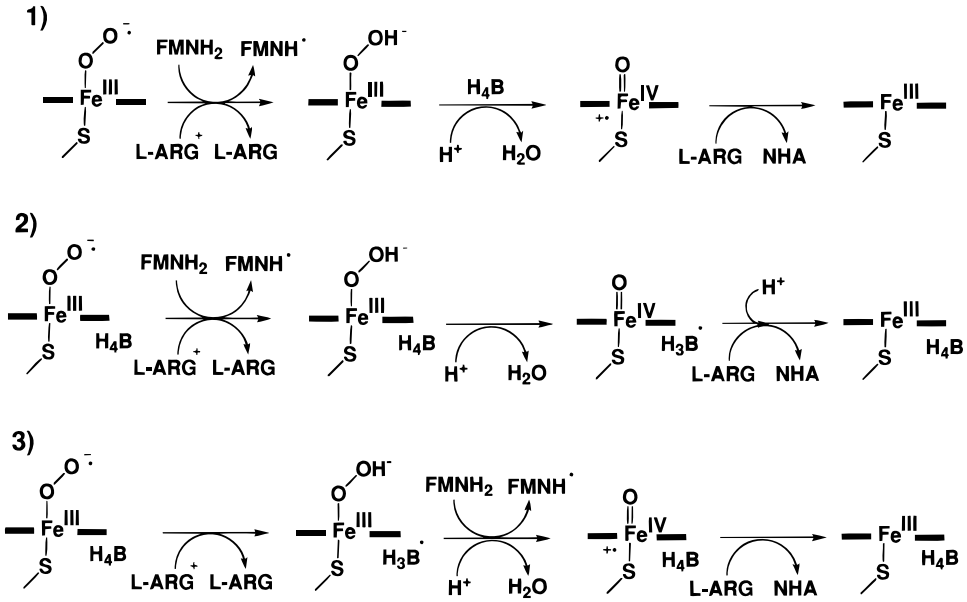

FIGURE 7: Three potential roles for H_4B in the conversion of L-Arg to NHA by NOS. In (1), H_4B mediates reactivity of the heme−oxygen complex, whereas in (2) and (3), H_4B acts as a redox-active cofactor for supplying an electron to the active center. In (2), an electron from H_4B participates directly in forming oxo-iron from peroxo-iron, whereas in (3), an electron from H_4B reduces superoxo-iron to peroxo-iron.

H_4B for NOS compared to neutral H_4B is not unlike the increased affinity of protonated methotrexate for dihydrofolate reductase (DHFR) compared to neutral folate (*73*−*75*). As with 4-amino-H_4B compared to H_4B, the substitution of the 4-oxo position in folate for an amine functionality in methotrexate raises the pterin pK_a and allows a different protonation state in the binary complex with DHFR (*73*−*75*). The interaction of methotrexate protonated N1 with the Asp27 carboxylate in DHFR (*76*) is much like the interaction of the 4-amino-H_4B with the NOS heme carboxylate. However, unlike the identical binding modes of 4-amino-H_4B and H_4B in NOS, protonated methotrexate binds DHFR with an 165° flip of the pterin ring compared to folate (*76*). Nevertheless, Asp27 favors protonation of bound pterins in ternary complexes with DHFR and $NADP^+$ (*73, 77*). Similarly, the NOS heme carboxylate likely favors the protonated form of 4-amino-H_4B. Because protonation of H_4B is not necessary for this interaction and its affinity for NOS is less than 4-amino-H_4B, H_4B likely binds NOS neutral, in contrast to the proposal of Raman et al. (*13*). The increased affinity on protonation is not seen with H_2B, which binds NOS ∼10× more weakly when compared to H_4B (*23*). This is consistent with the energetic cost of binding the proposed quinonoid form of H_2B, which is less stable than the dihydro form in free solution.

H_4B in the First Step of NOS Catalysis. On the basis of the three $iNOS_{ox}$ pterin complexes, we consider three possible functions for the pterin in the first step of NOS catalysis (Figure 7). In case 1, the pterin only influences the electronic state of the heme through its interaction with the heme carboxylate and sequestration of the proximal thiolate. Through these interactions, a change in pterin charge affects the reactivity of the heme−oxy complex, perhaps through an effect on the heme redox potential. In the second and third cases, pterin acts as an electron donor in the conversion of L-Arg to NHA, but at different stages of the reaction. In case 2, pterin supplies a reducing equivalent along with Fe(III) to form the high valent oxo-iron species after two exogenous electrons have already generated a peroxo-iron species. The resulting Fe(IV)oxo, $H_3B^\bullet$ radical would be analogous to the Fe(IV)oxo, $Trp^\bullet$ radical formed in compound I of cytochrome *c* peroxidase (CCP) (*78*). However, H_4B is 5.0 Å further from the NOS heme iron than the radical Trp is from the CCP heme iron. This mechanism also contrasts with cytochrome P-450 chemistry where the second oxidizing equivalent is thought to be localized to the iron−porphyrin−thiolate complex and in close proximity of the substrate. NOS could localize the radical farther from L-Arg to increase the stability of the activated oxygen species. In case 3, pterin supplies the second electron to the ferric−superoxy complex for formation of a precursor peroxo-iron intermediate (*21*) and then is replenished by $FMNH_2$ or $FMNH^\bullet$ (*65*)).

We suggest that H_4B likely binds to NOS in a neutral form and then oxidizes to a neutral radical during NOS catalysis. One-electron redox chemistry of H_4B has long been considered in NOS reactivity (*79*) and recently implicated in oxygen activation (*21*). Furthermore, formation of an $H_4B^{+\bullet}$ cation radical was suggested as the product of electron-transfer between the pterin and the heme based on L-Arg binding to the empty pterin site (*13*). Although a molybdopterin radical found in bacterial aldehyde dehydrogenases was also assumed to be a cation radical (*80*), one-electron oxidized tetrahydropterins characterized by EPR are often cation radicals because they are formed in acidic solutions (*81*−*85*). Kinetic studies of H_4B autoxidation indicate that ionization of the pterin 3,4-amide group greatly facilitates one-electron oxidation (*86*). Although the 3,4-amide in H_4B has a pK_a of ∼10, the value would be expected to be lower for $H_4B^{+\bullet}$ (*87*). In fact, spectroscopic titrations of tetrahydropterins with azide radicals suggest that ionization of the N3 amide group occurs between pH 7 and 10 (*87*). Moreover, interaction of the heme carboxylate with N3 would promote its deprotonation and interaction of a highly conserved Arg375 with O4 would stabilize negative charge developing on the pterin oxygen in the neutral radical (Figure 8). The ability of the heme carboxylate to catalyze conversion of 7,8-H_2B to q-H_2B (Figure 5B) would also support proton-transfer between the cofactors during catalysis. Thus, $H_4B^{+\bullet}$

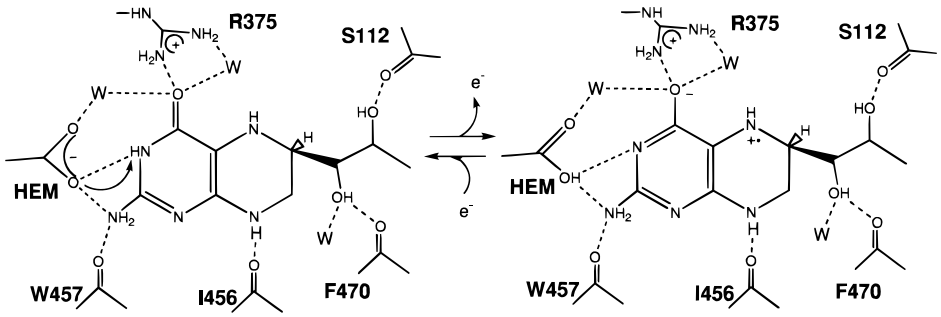

FIGURE 8: Possible proton-coupled electron-transfer during H_4B oxidation. The proton bound to H_4B N3 shifts to the heme carboxylate during pterin oxidation. The proposed positively charged state of 4-amino-H_4B may prevent this reaction from occurring.

may shift the proton at N3 to the heme carboxylate to produce a more stable $H_3B^{\bullet}$ species during or after oxidation (Figure 8). Stabilization of the negative charge on O4 may be reflected by detrimental catalytic effects of the R375A mutation in iNOS, which go beyond impairment of pterin binding or dimer stability (*40*). Surprisingly, mutation of the Arg375 equivalent in eNOS (R365) to Leu was reported to retain near native activity (*88*).

Taken together, the structure and biochemistry of these NOS-bound pterins suggest that for a redox function, H_2B inactivity can be explained by its dihydro oxidation state, while 4-amino-H_4B inactivity relates to its positive charge. Electrostatics argue that a protonated pterin should be less likely to oxidize. The one-electron oxidation potential of H_4B to $H_4B^{+\bullet}$ is already expected to be relatively low at neutral pH (< -300 mV (*66*)). The proposed positive charge on inactive 4-amino-H_4B will lower its oxidation potential further and limit its function as a redox-active cofactor in NOS. Although $H_4B^{+\bullet}$ can become neutral and effectively increase its oxidation potential by shifting the 3,4-amide proton to the heme carboxylate, 4-amino-$H_4B^{+\bullet}$ would still remain a cation.

H_4B in the Second Step of NOS Catalysis. In the second step of NOS catalysis, pterin redox activity is unnecessary, because dioxygen binding to the reduced heme produces the appropriate oxidation state (one-electron reduced oxygen) to form products. Nevertheless, in the absence of H_4B, iNOS converts NHA not to NO, but to NO^- (*89*), which is the same product formed when the second step is shunted with peroxide (two-electron reduced oxygen) (*54*). Furthermore, NO formation from N-hydroxyguanidines requires reaction with one-electron reduced oxygen, while NO^- formation requires reaction with two-electron reduced oxygen (*49*, *50*, *90*). This all suggests that in pterin-free NOS the superoxo−iron complex is reduced by the enzyme before it can react with NHA, which is consistent with increased rates of electron transfer from the reductase domain to the heme in the absence of pterin (*23*). H_4B binding could also modulate reactivity of the heme−oxygen complex in a manner that facilitates immediate reaction with NHA. Heme electronic sensitivity to pterin is supported by the increased heme redox potential of iNOS on binding H_4B (*91*). Additionally, given the structural coupling of the NHA site to the pterin site, the absence of pterin could alter the mode of NHA binding and its reactivity.

Finally, rates of proton delivery to heme-bound oxygen might also be be mediated by substrate. We originally proposed that differences between the ability of L-Arg and NHA to donate protons to the heme−oxygen complex may control oxygen activation (*12*). Proton abstraction from L-Arg by peroxo-iron would facilitate oxo-iron formation, whereas no proton would be available from neutral NHA for this function. Alternatively, L-Arg could protonate superoxo-iron, thereby raising the superoxo-iron redox potential and facilitating its further reduction. However, if NHA is protonated at physiological pH, it may also be capable of proton donation for oxygen activation. In this case, the mechanisms for the two steps of NOS catalysis would be distinguished by different reactivities of NHA and L-Arg toward similar heme oxygen species. Clearly, a delicate balance in the rates of electron and proton transfer to activated oxygen helps govern the products of NOS catalysis.

CONCLUSIONS

Structures of $iNOS_{ox}$ complexed with substrate L-Arg, intermediate NHA, or product analogue Scit, and with active or inactive pterins, provide new detailed structural information that limits possible mechanisms for NOS catalysis and suggests testable hypotheses for NOS cofactor function. The similar binding modes of L-Arg, NHA, and Scit adjacent to the heme iron suggest that heme-bound oxygen could catalyze both steps of NO synthesis without significant conformational rearrangement in the enzyme or substrate. L-Arg oxidation to NHA is likely to involve the putative oxo-iron species proposed for the similar chemistry of cytochrome P-450s. The L-Arg N^{ω} would be positioned well, relative to the heme iron, for reaction with oxo-iron. In the NHA complex, steric clash between heme-bound dioxygen and NHA suggests that either small structural shifts or a concerted reaction of dioxygen, NHA, and the reduced heme initiates the second step of NO synthesis. The structurally precluded interaction of the NHA hydroxyl with heme-bound oxygen rules against an initial hydrogen atom transfer between these species, but supports free radical addition of superoxo-iron to the NHA oxime or proton donation from protonated N^{ω} to the heme oxygen species. The NHA hydroxyl is directed into a pocket created between β-strands of the winged β-sheet fold that allows interaction with a peptide nitrogen and distortion of the hyroxyguanidinium plane by protonation and/or contact with the heme ring. These interactions may dispose NHA toward an Fe(III)−peroxo−NHA radical intermediate and catalyze its collapse to L-Cit and NO.

Our structures of active and inactive pterin analogues indicate that the pterin dependence of NO synthesis cannot be solely structural. H_2B inactivity can be due to its higher oxidation or protonation state relative to H_4B, while 4-amino-H_4B inactivity can only be due to its higher protonation state.

NOS likely binds H_4B in a neutral form based on its lower binding affinity compared to 4-amino-H_4B. The pterin likely acts as an electron donor in the first step of NO synthesis and as a mediator of heme reactivity in the second. We propose that H_4B shifts a proton from the 3,4-amide to the heme carboxylate to facilitate pterin oxidation and ability to act in rapid electron delivery. The oxidation of L-Arg to L-Cit and NO by NOS is a complicated reaction that crosses many different transition states. Remarkably, these reactions involve similar reactants and similar conformations of the same active center. Thus, the structure of the NOS active center channels the reactivity of heme, pterin, substrates, and activated oxygen through multiple steps of catalysis that are evidently not controlled by significantly different protein conformations. Instead, chemical control in NOS appears to depend on the intrinsic reactivity of the developing substrates and on the rates at which they trigger the transfer of protons and electrons in the NOS active center.

ACKNOWLEDGMENT

We thank the Advanced Light Source (ALS) and the Stanford Synchrotron Radiation Laboratory (SSRL) for use of data collection facilities, B. Mayer for 4-amino-H_4B, R. J. Rosenfeld for assistance with data collection, and A.M. Bilwes for helpful discussions.

NOTE ADDED IN PROOF:

An $H_3B^{\bullet}$ radical was recently identified during the reaction of $iNOS_{ox}$ with O_2 and L-Arg (*93*). The protonation state of the radical was not established.

REFERENCES

1. Stuehr, D. J., Kwon, N. S., Nathan, C. F., Griffith, O. W., Feldman, P. L., and Wiseman, J. (1991) *J. Biol. Chem. 266*, 6259.
2. Pfeiffer, S., Mayer, B., and Hemmens, B. (1999) *Angew. Chem., Int. Ed. Engl. 38*, 1715.
3. Griffith, O. W., and Stuehr, D. J. (1995) *Annu. Rev. Physiol. 57*, 707.
4. Masters, B. S. S., McMillan, K., Sheta, E. A., Nishimura, J. S., Roman, L. J., and Martasek, P. (1996) *FASEB J. 10*, 552.
5. Mueller, E. J., Loida, P. J., and Sligar, S. G. (1995) in *Cytochrome P450: Structure, Mechanism, and Biochemistry* (de Montellano, P. R. O., Ed.) pp 83−124, Plenum Press, New York, 1995.
6. Sono, M., Roach, M. P., Coulter, E. D., and Dawson, J. H. (1996) *Chem. Rev. 96*, 2841.
7. Stuehr, D. J., Sapse, A. M., and Sapse, D. S. (1993) *Struct. Chem. 4*, 143.
8. Korth, H.-G., Sustmann, R., Thater, C., Butler, A. R., and Ingold, K. U. (1994) *J. Biol. Chem. 269*, 17776.
9. Feldman, P. L., Griffith, O. W., Hong, H., and Stuehr, D. J. (1993) *J. Med. Chem. 36*, 491.
10. Marletta, M. (1994) *J. Med. Chem. 37*, 1899.
11. Stuehr, D. J. (1997) *Annu. Rev. Pharmacol. Toxicol. 18*, 707.
12. Crane, B. R., Arvai, A. S., Ghosh, D. K., Wu, C., Getzoff, E. D., Stuehr, D. J., and Tainer, J. A. (1998) *Science 279*, 2121.
13. Raman, C. S., Li, H., Martasek, P., Kral, V., Masters, B. S. S., and Poulos, T. L. (1998) *Cell 95*, 939.
14. Fischmann, T. O., Hruza, A., Niu, X. D., Fossetta, J. D., Lunn, C. A., Dolphin, E., Prongay, A. J., Reichert, P. R., Lundell, D. J., Narula, S. K., and Weber, P. C. (1999) *Nat. Struct. Biol. 6*, 233.
15. Li, H., Raman, C. S., Glaser, C. B., Blasko, E., Young, T. A., Parkinson, J. F., Whitlow, M., and Poulos, T. L.(1999) *J. Biol. Chem. 30*, 21276.
16. Marletta, M. A., Hurshman, A. R., and Rusche, K. M. (1998) *Curr. Op. Chem. Biol. 2*, 656.
17. Baek, K. J., Thiel, B. A., Lucas, S., and Stuehr, D. J. (1993) *J. Biol. Chem. 268*, 21120.
18. Gorren, A. C. F., List, B. M., Schrammel, A., Pitters, E., Hemmens, B., Werner, E. R., Schmidt, K., and Mayer, B. (1996) *Biochemistry 35*, 16735.
19. Gorren, A. C. F., Schrammel, A., Schmidt, K., and Mayer, B. (1998) *Biochem. J. 331*, 801.
20. Toth, M., Kukor, Z., and Sahin-Toth, M. (1998) *Mol. Hum. Reprod. 4*, 1165.
21. Bec, N., Gorren, A. C. F., Voelker, C., Mayer, B., and Lange, R. (1998) *J. Biol. Chem. 273*, 13502.
22. Klatt, P., Schmid, M., Leopold, E., Schmidt, K., Werner, E. R., and Mayer, B. (1994) *J. Biol. Chem. 269*, 13861.
23. Presta, A., Siddhanta, U., Wu, C., Sennequier, N., Huang, L. X., Abu-Soud, H. M., Erzurum, S., and Stuehr, D. J. (1998) *Biochemistry 37*, 298.
24. Werner, E. R., Pitters, E., Schmidt, K., Watcher, H., Werner-Felmayer, G., and Mayer, B. (1996) *Biochem J. 320*, 193.
25. Ghosh, D. K., Wu, C., Pitters, E., Moloney, M., Werner, E. R., Mayer, B., and Stuehr, D. J. (1997) *Biochemistry 36*, 10609.
26. Otwinowski, Z. (1993) in *Data Collection and Processing* (Sawyer, L., Isaacs, N., and Bailey, S., Eds.) pp 56−62, Science and Engineering Research Council, Warrington, U.K.
27. McRee, D. E. (1999) *J. Struct. Biol. 125*, 156.
28. Brünger, A. T., Kuriyan, J., and Karplus, M. (1987) *Science 235*, 458.
29. Brunger, A. T., Adams, P. D., Clore, G. M., DeLano, W. L., Gros, P., Grosse-Kunstleve, R. W., Jiang, J. S., Kuszewski, J., Nilges, M., Pannu, N. S., Read, R. J., Rice, L. M., Simonson, T., and Warren, G. L. (1998) *Acta Crystallogra D54*, 905.
30. Miller, M. A., Shaw, A., and Kraut, J. (1994) *Nat. Struct. Biol. 1*, 524.
31. Loew, G. H., Harris, D. L., and Dupuis, M. (1997) *J. Mol. Struct. 398*, 497.
32. Harris, D. L., and Loew, G. H. (1996) *J. Am. Chem. Soc. 118*, 10588.
33. Friant, P., Goulon, J., Fischer, J., Ricard, L., Schappacher, M., Weiss, R., and Momenteau, M. (1985) *New J. Chem. 9*, 33.
34. Burstyn, J. N., Roe, J. A., Miksztal, A. R., Shaevitz, B. A., Lang, G., and Valentine, J. S.(1988) *J. Am. Chem. Soc. 110*, 1382.
35. Selke, M., and Valentine, J. S. (1998) *J. Am. Chem. Soc. 120*, 2652.
36. Harris, D. L. and Loew, G. H. (1998) *J. Am. Chem. Soc. 120*, 8941.
37. Crane, B. R., Arvai, A. S., Gachhui, R., Wu, C., Ghosh, D. K., Getzoff, E. D., Stuehr, D. J., and Tainer, J. A. (1997) *Science 278*, 425.
38. Doubell, P. C. J., Oliver, D. W., and Rooyen, P. H. (1991) *Acta Crystallogr. C47*, 353.
39. Larson, I. K. (1975) *Acta Crystallogr. B31*, 1626.
40. Ghosh, S., Wolan, D., Adak, S., Crane, B. R., Kwon, N. S., Tainer, J. A., Getzoff, E. D., and Stuehr, D. J. (1999), *J. Biol. Chem. 274*, 24100.
41. Brown, D. J. (1998) in *The Chemistry of Heterocyclic Compounds*, Brown, D., Ed. Vol. 24, John Wiley and Sons, New York.
42. Kwon, N. S., Nathan, C. F., Gilker, C., Griffith, O. W., Mathews, D. E., and Stuehr, D. J. (1990) *J. Biol. Chem. 265*, 13442.
43. Leone, A. M., Palmer, R. M. J., Knowles, R. G., Francis, P. L., Ashton, D. S., and Moncada, S. (1991) *J. Biol. Chem. 266*, 23790.
44. Abu-Soud, H. M., Presta, A., Mayer, B., and Stuehr, D. J. (1997) *Biochemistry 36*, 10810.
45. Clement, B., Schultzemosgau, M. H., and Wohlers, H. (1993) *Biochem. Pharm. 46*, 2249.
46. Jousserandot, A., Boucher, J. L., Henry, Y., Niklaus, B., Clement, B., and Mansuy, D. (1998) *Biochemistry 37*, 17179.

47. Clement, B., Boucher, J. L., Mansuy, D., and Harsdorf, A. (1999) *Biochem. Pharm. 58*, 439.
48. Sennequier, N., Boucher, J. L., Battinoi, P., and Mansuy, D. (1995) *Tetrahedron Lett. 36*, 6059.
49. Fukuto, J. (1996) *Methods Enzymol. 268*, 365.
50. Fukuto, J. M., Stuehr, D. J., Feldman, P. L., Bova, M. P., and Wong, P. (1993) *J. Med. Chem. 36*, 2666.
51. Tierney, D. L., Huang, H., Martasek, P., Masters, B. S. S., Silverman, R. B., and Hoffman, B. M. (1999) *Biochemistry 38*, 3704.
52. Roman, L. J., Sheta, E. A., Martasek, P., Gross, S. S., Liu, Q., and Masters, B. S. S. (1995) *Proc. Natl. Acad. Sci. U.S.A. 92*, 8428.
53. Mansuy, D., Boucher, J. L., and Clement, B. (1995) *Biochimie 77*, 661.
54. Clague, M. J., Wishnok, J. S., and Marletta, M. A. (1997) *Biochemistry 36*, 14465.
55. Tzeng, E., Billiar, T. R., Robbins, P. D., Loftus, M., and Stuehr, D. J. (1995) *Proc. Natl. Acad. Sci. U.S.A. 92*, 11771.
56. Ghosh, D. K., Abu-Soud, H. M., and Stuehr, D. J. (1996) *Biochemistry 35*, 1444.
57. Presta, A., Siddhanta, U., Wu, C., Sennequier, N., Huang, L., Abu-Soud, H. M., Erzurum, S., and Stuehr, D. J. (1997) *Biochemistry 37*, 298.
58. Rodriguez-Crespo, I., Gerber, N. C., and de Montellano, P. R. O. (1996) *J. Biol. Chem. 271*, 11462.
59. Sahin-Toth, M., Kukor, Z., and Toth, M. (1997) *Mol. Hum. Reprod. 3*, 293.
60. Huang, L., Abu-Soud, H. M., Hille, R., and Stuehr, D. J. (1999) *Biochemistry 38*, 1912.
61. Green, M. T. (1999) *J. Am. Chem. Soc. 121*, 7939.
62. Pfeiffer, S., Gorren, A. C. F., Pitters, E., Schmidt, K., Werner, E. R., and Mayer, B. (1997) *Biochem J. 328*, 349.
63. Mayer, B., Wu, C. Q., Gorren, A. C. F., Pfeiffer, S., Schmidt, K., Clark, P., Stuehr, D. J., and Werner, E. R. (1997) *Biochemistry 36*, 8422.
64. Riethmuller, C., Gorren, A. C. F., Pitters, E., Hemmens, B., Habisch, H. J., Heales, S. J. R., Schmidt, K., Werner, E. R., and Mayer, B. (1999) *J. Biol. Chem. 274*, 16047.
65. Witteveen, C. F. B., Giovanelli, J., Yim, M. B., Gachhui, R., Stuehr, D. J., and Kaufman, S. (1998) *Biochem. Biophys. Res. Comm. 250*, 36.
66. Eberlein, G., Bruice, T. C., Lazarus, R. A., Henrie, R., and Benkovic, S. J. (1984) *J. Am. Chem. Soc. 106*, 7916.
67. Witteveen, C. F. B., Giovanelli, J., and Kaufman, S. (1996) *J. Biol. Chem. 271*, 4143.
68. Armarego, W. L. F., Randles, D., and Taguchi, H. (1983) *Eur. J. Biochem. 135*, 393.
69. Armarego, W. L. F., and Waring, P. (1982) *J. Chem. Soc., Perkin Trans. 2 10*, 1227.
70. Archer, M. C., and Scrimgeour, K. G. (1970) *Can. J. Biochem. 48*, 278.
71. Kaufman, S. (1967) *J. Biol. Chem. 242*, 3934.
72. Kappock, T. J., and Caradonna, J. P. (1996) *Chem. Rev. 96*, 2659.
73. Chen, Y., Kraut, J., Blakley, R. L., and Callender, R. (1981) *Biochemistry 33*, 7021.
74. Blakley, R. L., and Cocco, L. (1985) *Biochemistry 24*, 4704.
75. Cocco, L., Groff, J. P., Temple, C., Montgomery, J. A., London, R. E., Matwiyoff, N. A., and Blakley, R. L. (1981) *Biochemistry 24*, 3972.
76. Bystroff, C., Oatley, S., and Kraut, J. (1990) *Biochemistry 29*, 3263.
77. Howell, E. E., Villafranca, J. E., Warren, M. S., Oatley, S. J., and Kraut, J. (1986) *Science 231*, 1123.
78. Sivaraja, M., Goodin, D. B., Smith, M., and Hoffman, B. M. (1989) *Science 245*, 738.
79. Mayer, B., and Werner, E. R. (1995) *Nauyn. Arch. of Pharm. 351*, 453.
80. Luykx, D. M. A. M., Duine, J. A., and de Vries, S. (1998) *Biochemistry 37*, 11366.
81. Bobst, A. (1967) *Helv. Chim. Acta 50*, 2222.
82. Bobst, A. (1968) *Helv. Chim. Acta 51*, 607.
83. Ehrenberg, A., Mager, P., Müller, P., Okada, T., and Viscontini, M. (1967) *Helv. Chim. Acta 50*, 411.
84. Westerling, J., Mager, H. I. X., and W., B. (1977) *Tetrahedron 51*, 2587.
85. Funahashi, Y., Kohzuma, T., Odani, A., and Yamauchi, O. (1994) *Chem. Lett. 2*, 385.
86. Blair, J. A., and Pearson, A. J. (1974) *J. Chem. Soc., Perkin Trans. 2*, 80.
87. Armstrong, D. A., Farahani, M., and Surdhar, P. S. (1990) *Can. J. Chem. 68*, 1974.
88. Chen, P., Berka, V., Tsai, A., and Wu, K. (1999) *J. Biol. Chem. 273*, 34164.
89. Rusche, K. M., Spiering, M. M., and Marletta, M. A. (1998) *Biochemistry 37*, 15503.
90. Yoo, J., and Fukuto, J. M. (1995) *Biochem. Pharm. 50*, 1995.
91. Presta, A., Weber-Main, A. M., Stankovich, M. T., and Stuehr, D. J. (1998) *J. Am. Chem. Soc. 120*, 9460.
92. Boggs, S., Huang, L., and Stuehr, D. J. (2000) *Biochemistry* (in press).
93. Hurshman, A. R., Krebs, C., Edmondson, D. E., Huynh, B. H., and Marletta, M. A. (1999) *Biochemistry 38*, 15689.

BI992409A